Dynamic Performance Improving Sliding-Mode Control-Based Feedback Linearization for PV System Under LVRT Condition

Yajing Zhang, Jing Wang, Hong Li, *Senior Member, IEEE*, Trillion Q. Zheng, *Senior Member, IEEE*, Jih-Sheng Lai, *Fellow, IEEE*, Jianguo Li, Jiuhe Wang, and Qian Chen

***Abstract*—The low-voltage ride through condition (LVRT) attracts wider attention with the increased power of central grid-connected photovoltaic (PV) systems. The conventional double-loop-based control strategy designed for the nominal voltage is slow and potentially unstable under the LVRT operation. In this article, a novel sliding-mode control-based feedback linearization is proposed to improve response speed of the PV system under LVRT condition. To increase the robustness of the control to parameter variations, sliding-mode control is combined with the feedback linearization in this article. Further, the complete linearization of the PV system can be achieved over the whole operating range. Moreover, the dc-link voltage operating point of the PV panel can be dynamically adjusted based on the drop depth of the grid voltage, which will reduce the load changes during the LVRT and subsequently ensure the ac current levels to stay within the design limits in any fault situation and enhance the LVRT capability of the central grid-connected PV system. Finally, a 100-kW PV inverter is built to validate the feasibility and effectiveness of the proposed strategy for LVRT.**

***Index Terms*—Solar energy, photovoltaic power systems, pulse width modulated inverters, nonlinear systems, optimization methods.**

Manuscript received September 4, 2019; revised December 26, 2019; accepted March 16, 2020. Date of publication March 30, 2020; date of current version July 20, 2020. This work was supported in part by the Natural Science Foundation of Beijing under Grants 3204040 and 3202010, in part by the Key Science and Technology Projects of China Southern Power Grid Corporation under Grant 090000KK52180116, in part by the National Natural Science Foundation of China under Grant 51777012 and 51477011, and in part by the Natural Science Foundation of Beijing – Education Committee Joint Funding Project under Grant KZ201911232045. This article is an extension of a conference paper, "Application of feedback linearization strategy in voltage fault ride-through for photovoltaic inverters," in *Proc. IEEE Conference on Industrial Electronics Society (IECON 2011)*, Oct. 2011. Recommended for publication by Associate Editor M. Ordonez. *(Corresponding author: Yajing Zhang.)*

Yajing Zhang, Jianguo Li, and Jiuhe Wang are with the School of Automation, Beijing Information Science and Technology University, Beijing 100192, China (e-mail: zhangyajing@bistu.edu.cn; lijianguo@bistu.edu.cn; wjhyhrwm@163.com).

Jing Wang is with the Shenzhen Power Supply Bureau Co., Ltd., Shenzhen 518053, China (e-mail: 489671806@qq.com).

Hong Li and Trillion Q. Zheng are with the School of Electrical Engineering, Beijing Jiaotong University, Beijing 100044, China (e-mail: hli@bjtu.edu.cn; tqzheng@bjtu.edu.cn).

Jih-Sheng Lai is with the Electrical and Computer Engineering Department, Virginia Polytechnic Institute & State University, Blacksburg, VA 24061-0111 USA (e-mail: laijs@vt.edu).

Qian Chen is with the Zhejiang Electric Power Corporation Research Institute, Hangzhou 310014, China (e-mail: chenqian05291148@126.com).

Color versions of one or more of the figures in this article are available online at https://ieeexplore.ieee.org.

Digital Object Identifier 10.1109/TPEL.2020.2983315

I. Introduction

PHOTOVOLTAIC (PV) power generation systems have great benefits to deal with the environmental challenges, which has attracted wider attention in the past decades [1], [2]. As the proportion of PV power generation systems in the electrical power systems increases, the stability and safety of power grid are now facing significant challenge mainly due to the randomness and volatility of the PV system [3]. The power system requires more stable and more reliable characteristics of the PV power generation systems and better quality generated by them [4], [5].

Recently, the medium-voltage grid standards such as IEEEP1547.8, DIN/VDE0126-1-1, UL1741, and G83/1 have been drafted, which require that the PV systems have low-voltage ride through (LVRT) capability [6]–[8]. With the improvement of LVRT performance requirements, the PV system should continue to connect and contribute to the electrical power system, and keep the grid voltage and frequency stable under the LVRT condition. The profile of LVRT code (GB/T 19964) used in China is shown in Fig. 1. The required performance for the PV is as follows.

1) When the voltage of the grid falls to zero, the PV system should remain connected for a minimum time duration of 150 ms.
2) When the grid voltage falls below the red line, the PV system could be cut off from the grid.
3) After the grid voltage returns to normal value, the PV system should restore to the rated power. The power recovery speed should not be less than 30% of the rated power per second.

The control technique of the PV systems faces the challenge for the uncertainty of the input power [9]–[11]. In general, the traditional double-loop control based on stationary reference with pulsewidth modulation (PWM) is used in three-phase PV inverter [12], [13]. It is difficult to obtain theoretical evidence of strict stability and tracking performance over the entire operating range, because the dynamic equations of the three-phase PV inverter have nonlinear characteristics. During LVRT, the system's state can be significantly far away from the desired operating point, the traditional linear controllers will result in slow response, and they could not guarantee satisfactory dynamic response [14]. Consequently, it may cause an LVRT failure, such

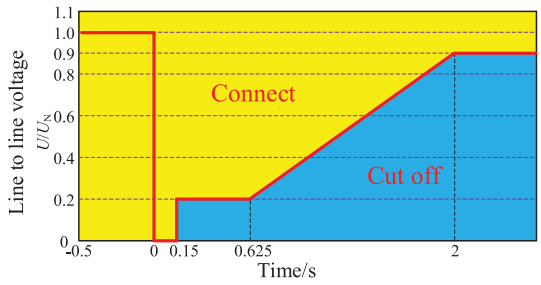

Fig. 1. Voltage duration profile of GB/T 19964.

as the abrupt current spike which will exceed three times or more of the rated current, the sudden surge of the dc-link voltage due to unbalanced condition of input and output power [15].

The improved control strategy based on classic multi-loop controllers has been proposed to improve LVRT capability of the PV system [14]–[17]. The LVRT is handled by using additional cascaded loops. However, it could not fundamentally solve slow dynamic response problem of the system. A dynamical power limiter was used to limit the current of the inverter, but its reference current can be saturated [18], [19].

Many strategies for improving system robustness have been proposed [20]–[22]. A robust fuzzy controller based on Taguchi-tuning approach is presented in [23]–[25], which will improve the stabilization of the grid-connected PV system. A sliding-mode control method was adopted in the LVRT application [26], [27]. The controller considered the uncertainties and the sudden surge of the dc-link voltage, keeping the ac current within tolerances [26]. However, experiment verifications of deep voltage drop are not given and the grid voltage and power level are far different from the actual situation. Adaptive control strategy has been proposed to solve LVRT problems in PV system [28]. A predictive power control method was proposed in [29]–[31], which could provide suitable energy under disturbances. To improve robustness on parameter variation, a H-inf control method was used in wind application [32].

Feedback linearization technique is one of the advanced and efficient control schemes to handle with the nonlinearity problem [33]–[37]. In [33], the feedback linearization technique is used to solve the mismatch voltages between the fuel cell and the vehicles. Small signal of the wide voltage-gain dc–dc converter is established based on feedback linearization method. By adopting the method of transformation and feedback, the feedback linearization technique could obtain a linear relation between the inputs and the outputs of the system. Thus, it could predict the response of the system over the whole operating range and obtain desired dynamic performances [36]. A feedback linearization strategy is first applied in PV system, and the current controller is linearized to improve the behavior of the system [38]. However, this method is unpractical due to excessive number of sensors and difficult mathematical operations. A simple feedback linearizing controller was proposed in [39], where both power factor and dc-link voltage were controlled by this method. However, this controller only considered the power balance dynamics by sensing the voltage of the dc-link capacitor, but not considered the nonlinear switching functions of the inverter. Therefore, this method is not completely linearized. In [40], a feedback linearizing method was applied to improve the behavior of the inner current-loop controller of the PV system, but the dc-link voltage reference is still constant without considering the PV array's special characteristics. Therefore, the control model cannot accurately describe the true system, which will lead to stability problems. The feedback linearization technique has also been applied in other topologies; for example, wind power system [41], micro-inverters [42], dual-stage grid-tied inverters [43], [44] and z source inverter [45]. In [41], feedback linearization combined with sliding-mode approach was applied in the wind turbine. It focused on the dc-link overvoltage and overcurrent in the rotor circuit and it also validated the feasibility of the feedback linearization method in LVRT applications. However, the improvements in experimental verification are needed to further verify its effectiveness. In [43], direct power control strategy based on feedback linearization was proposed to regulate the active and reactive powers of the dual-stage inverter. This approach achieved a good dynamic response under unbalanced grid voltages. But there are few discussions about the performance of depth drop required for LVRT.

This article is organized as follows. In Section II, the modeling of the central grid-connected PV system and the characterization of voltage dip during grid fault are briefly reviewed. In Section III, the proposed sliding-mode based feedback linearization controller is set out. In Section IV, comparison simulations and experimental results with traditional proportional integral (PI) double-loop control strategy are provided and discussed to show the effectiveness of the proposed control strategy. Finally, Section V presents the conclusions of this work.

A basic idea of the proposed sliding-mode based feedback linearization controller for the PV system was proposed in a conference article [37] by the authors. This article is the further and comprehensive study to assist LVRT operation of the grid-connected PV system. A close observation indicates that the main contributions of this article include the following.

1) The proposed feedback linearization controller is further improved by combining with sliding-mode compensator, and more detailed discussion, model, and formula are presented.
2) Completed decoupling and linearization over the entire operating range and fast dynamic response of LVRT are realized through the proposed approach.
3) The dc-link voltage operating point is considered to reduce the imbalance of the input and output power during the LVRT.
4) Both symmetrical and asymmetrical LVRTs are compared through simulations and experimental verifications with traditional PI double-loop control strategy.

II. Central Grid-Connected PV System

A. Three-Phase Central Grid-Connected PV System

The single-stage central grid-connected PV system includes a PV module, a three-phase single-stage voltage source inverter, a transformer, and a three-phase grid source, as shown in Fig. 2. Where T_1–T_6 are the main power switches of the inverter, C

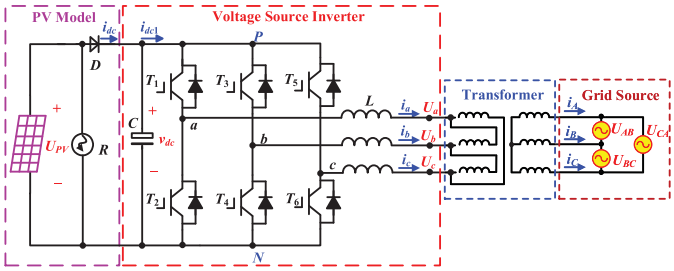

Fig. 2. Single-stage topological structure of the central grid-connected PV system.

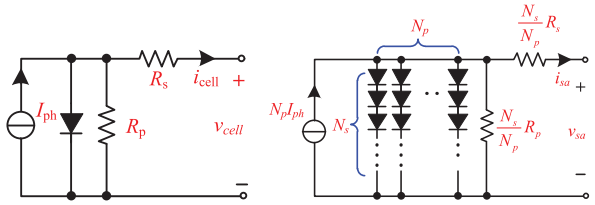

Fig. 3. Equivalent circuit of PV cell and PV array. (a) PV cell. (b) PV array.

is the dc-link capacitor, and L is the three-phase inductance of the ac side. $i_{\rm dc}$ and $i_{\rm dc1}$ are the currents before and after the dc-link capacitor, and $v_{\rm dc}$ is the voltage of the dc-link capacitor. i_a, i_b, and i_c are currents of the three-phase inductor, and U_a, U_b, and U_c are primary-side three-phase voltage of the transformer. U_{AB}, U_{BC}, and U_{CA} are the line voltage of the grid.

An equivalent circuit of the PV cell and PV array is depicted in Fig. 3. Usually, a current source I_{ph} in parallel with a diode is used to represent the ideal PV cell. However, the PV cells are not ideal in practical applications. Then, a parallel resistance R_p and a series resistance R_s are added to the PV cell model, as shown in Fig. 3(a). The PV array model is shown in Fig. 3(b). N_s represents the number of PV cells in series, and N_p represents the number of PV cells in parallel. Using the standard equations, the output current of the PV array can be obtained [46]

$$i_{sa} = N_p I_{ph} - N_p I_s \left[\exp\left[\alpha\left(\frac{v_{sa}}{N_s} + \frac{R_s i_{sa}}{N_p}\right)\right] - 1\right] - \frac{N_p}{R_p}\left(\frac{v_{sa}}{N_s} + \frac{R_s i_{sa}}{N_p}\right) \tag{1}$$

where I_s is the saturation current of the PV cell, I_{sa} and v_{sa} are the output current and output voltage of the PV array. Where $\alpha = q/AkT_c$. The q, A, and k are elementary charge, ideal factor of the p–n junction, and Boltzmann's constant, respectively. The I/V and P/V characteristics of the PV array at standard test condition (STC) are given in Fig. 4. The maximum power point (MPP) at STC is chosen as 600 V at a rated current of 167 A leading to a power of 100 kW. The system voltage U_{oc} is chosen as state-of-the art to 670 V with a short-circuit current $I_{\rm sc}$ of 190 A, based on the G3-1090X model of Emcore company.

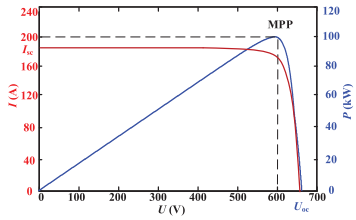

Fig. 4. I/V and P/V characteristics of PV array at STC (temperature of 25°C, spectrum of light equals 1.5 air mass, irradiation 1000 W/m^2).

B. Classification of Voltage Dip During LVRT

Voltage dip is an event in which the root mean square (rms) voltage of the grid drops suddenly in a short period of time. The typical duration is 0.5–30 cycles [47]. In the analysis of the voltage dip, the ratio of the rms grid voltage of the dip to the rms value of the normal grid voltage is usually defined as the magnitude of the drop, and the time between the occurrence and the end of the fall is defined as the duration. Voltage dips are often accompanied by sudden changes in the voltage phase, referred as phase jumps [48].

Past power system operation experience showed that most voltage dips belong to asymmetrical faults. The ratio of single-line-to-ground grid voltage dips are 68%, two-lines-to-ground voltage dips are 21%, and three-phase voltage dips are 11% [49], [50]. For asymmetric grid voltage dips, the grid voltage vector contains not only the fundamental component but also the negative sequence component or even the zero-sequence component [48]. It is generally assumed that the line impedances of the positive sequence component, the zero-sequence component, and the negative sequence component are equal [51].

III. Implementation of the Proposed Sliding-Mode-Based Feedback Linearization Controller

A. Feedback Linearization of the Three-Phase PV System

The feedback linearization theory for nonlinear multi-input multi-output system is described in [26]. The main idea of the feedback linearization is to design a nonlinear controller using transformation and feedback method. Hence, the nonlinear system will transform into a fully or partially decoupled linear system. After that, desired dynamic control techniques can be easily applied on the system.

Before applying the nonlinear control to the central grid-connected PV system, the d–q rotating coordinates model of the system should be given first, as follows:

$$L\frac{di_d}{dt} = e_d + \omega L i_q - R i_d - v_d \tag{2}$$

$$L\frac{di_q}{dt} = e_q - \omega L i_d - R i_q - v_q \tag{3}$$

$$C\frac{dv_{\rm dc}}{dt} = i_{\rm dc} - i_{\rm dc1}. \tag{4}$$

We select the d-axis as the reference frame of the grid voltage synthesis vector in the *park* transformation, where i_d, i_q, e_d, and e_q are currents and voltage vectors of the ac side in the d–q

rotating reference frame, v_d and v_q are the d–q rotating reference frame vectors of the inverter output voltage, $v_{\rm dc}$ is the dc-link voltage; *R* and *L* represent the total resistance and inductance between the terminals of the grid-connected transformer and the PV power inverter, and *C* stands for the capacitance in the dc-link. Equations (2)–(4) can be rewritten as a matrix as follows:

$$\begin{pmatrix} \dot{i}_d \\ \dot{i}_q \\ \dot{v}_{\rm dc} \end{pmatrix} = \begin{pmatrix} \frac{1}{L}e_d - \frac{R}{L}i_d + \omega i_q \\ \frac{1}{L}e_q - \frac{R}{L}i_q - \omega i_d \\ \frac{1}{C}i_{dc} - \frac{3}{2Cv_{\rm dc}}(e_d i_d) \end{pmatrix} + \begin{pmatrix} -\frac{1}{L} \\ 0 \\ 0 \end{pmatrix} v_d + \begin{pmatrix} 0 \\ -\frac{1}{L} \\ 0 \end{pmatrix} v_q. \tag{5}$$

For the design of the input–output feedback linearization control law of the PV system, the nonlinear multivariable dynamic model of the studied system defined by (5) can be expressed in the classical form of nonlinear system [52]

$$\dot{x} = f(x) + G(x)u \tag{6}$$

$$y = h(x) \tag{7}$$

where *x* stands for the state variables matrix, *y* stands for the output vectors matrix, and *u* stands for the input vectors matrix of the nonlinear PV system

$$f(x) = \begin{pmatrix} \frac{1}{L}e_d - \frac{R}{L}i_d + \omega i_q \\ \frac{1}{L}e_q - \frac{R}{L}i_q - \omega i_d \\ \frac{1}{C}i_{\rm dc} - \frac{3}{2Cv_{\rm dc}}(e_d i_d) \end{pmatrix} \tag{8}$$

$$g(x) = \begin{pmatrix} -\frac{1}{L} & 0 \\ 0 & -\frac{1}{L} \\ 0 & 0 \end{pmatrix} \tag{9}$$

$$x = \begin{bmatrix} i_d & i_q & v_{\rm dc} \end{bmatrix}^T \tag{10}$$

$$y = h(x) \tag{11}$$

$$u = \begin{bmatrix} v_d & v_q \end{bmatrix}^T. \tag{12}$$

Because there are two independent inputs, two outputs need to be decoupled. The system has five variables, including i_d, i_q, v_d, v_q, and $v_{\rm dc}$. These variables could be divided into *d* variables and *q* variables. The *d* variables are i_d, v_d, and $v_{\rm dc}$, and the *q* variables are i_q and v_q. In the grid-connected PV system, the first task is to achieve maximum power tracking by adjusting the dc-link voltage. Thus, we choose the $v_{\rm dc}$ as one of the outputs. The second task is to regulate the power factor of the ac current. The variable i_q could directly reflect the power factor. Therefore, another output variable selects i_q

$$\begin{cases} y_1 = h_1(x) = i_q \\ y_2 = h_2(x) = v_{\rm dc}. \end{cases} \tag{13}$$

In order to obtain accurate input–output feedback linearization, the most basic way is to obtain the input variables by differentiating the output y_i until the input variables appear and then the nonlinearity could be eliminated by designing the input variables. Lie derivative simplification method is used in the derivation process. Assume that r_i is the smallest integer, then the input variables will appear in the in the r_ith derivation of y_i

$$y_i^{r_i} = L_f^{r_i} h_i + \sum_{j=1}^{m} L_{gi} L_f^{r_i - 1} h_i u_j \tag{14}$$

where the relative degree of the output vector y_i is r_i and

$$L_{gi} L_f^{r_i - 1} h_i \neq 0. \tag{15}$$

According to this simplification method, the Lie derivative of function *h* relative to vector *f* is defined as

$$L^n{}_f h = (\partial L^{n-1}{}_f h / \partial x) f. \tag{16}$$

Especially, when r_i is equal to zero, we can prove that

$$L^0{}_f h = h. \tag{17}$$

Performing the Lie derivative process above for each output yields

$$\begin{aligned} \dot{y}_1 &= L_f h_1 + (L_{g1} h_1) u_1 + (L_{g2} h_1) u_2 \\ &= \frac{1}{L} e_q - \frac{R}{L} i_q - \omega i_d - \frac{1}{L} u_2 \end{aligned} \tag{18}$$

$$\begin{aligned} \dot{y}_2 &= L_f h_2 + (L_{g1} h_2) u_1 + (L_{g2} h_2) u_2 \\ &= \frac{1}{C} i_{\rm dc} - \frac{3}{2Cv_{\rm dc}} (e_d i_d). \end{aligned} \tag{19}$$

From (18) and (19), it can be seen that $L_{g1}h_2 = 0$ and $L_{g2}h_2 = 0$ and the input u_2 appears in the first derivative. The relative degree value of output y_1 is $r_1 = 1$. However, the input control variables of u_1 have not yet appeared, so differentiate again. The second-order derivative of y_2 can be calculated

$$\begin{aligned} \ddot{y}_2 &= L_f (L_f h_2) + L_{g1} (L_f h_2) u_1 + L_{g2} (L_f h_2) u_2 \\ &= -\frac{3e_d}{2Cv_{\rm dc}} \left(\frac{1}{L} e_d - \frac{R}{L} i_d + \omega i_q - \frac{1}{L} u_1 \right) \\ &\quad + \frac{3 i_d e_d}{2Cv_{\rm dc}^2} \left(\frac{3}{2Cv_{\rm dc}} (e_d i_d) - \frac{1}{C} i_{\rm dc} \right) + \frac{1}{C} \dot{i}_{\rm dc}. \end{aligned} \tag{20}$$

For output y_2, the relative degree is $r_2 = 2$. These equations may be rewritten as a matrix

$$\begin{bmatrix} \dot{y}_1 \\ \ddot{y}_2 \end{bmatrix} = A(t) + E(t) \begin{bmatrix} u_1 \\ u_2 \end{bmatrix} \tag{21}$$

where

$$\begin{aligned} E(t) &= \begin{bmatrix} L_{g1} h_1 & L_{g2} h_1 \\ L_{g1} L_f h_2 & L_{g2} L_f h_2 \end{bmatrix} \\ &= \begin{pmatrix} 0 & -\frac{1}{L} \\ \frac{3e_d}{2CLv_{\rm dc}} & 0 \end{pmatrix} \end{aligned} \tag{22}$$

$$\begin{aligned} A(t) &= \begin{bmatrix} L_f h_1 & L^2{}_f h_2 \end{bmatrix}^T \\ &= \begin{bmatrix} \frac{1}{L} e_q - \frac{R}{L} i_q - \omega i_d \\ -\frac{3e_d (\frac{e_d}{L} - \frac{R}{L} i_d + \omega i_q)}{2Cv_{\rm dc}} + \frac{3e_d i_d (\frac{3e_d i_d}{2Cv_{\rm dc}} - \frac{i_{\rm dc}}{C})}{2Cv^2{}_{\rm dc}} - \frac{\dot{i}_{\rm dc}}{C} \end{bmatrix}. \end{aligned} \tag{23}$$

Since

$$\det(E(t)) = \frac{3ed}{2L^2Cv_{\rm dc}} \neq 0. \tag{24}$$

The total relative degree of the system ($r_1 + r_2 = 3$) is equal to the system's order. So, there is no zero dynamics and complete linearization of the PV system is obtained by using

$$\begin{bmatrix} u_1 \\ u_2 \end{bmatrix} = E^{-1}\left[-A + \begin{bmatrix} \dot{y}_1 \\ \ddot{y}_2 \end{bmatrix}\right]. \tag{25}$$

B. Sliding-Mode-Based Feedback Linearization of the Central Grid-Connected PV System

The sliding-mode control method [23] makes the sliding trajectory of the variable always on the sliding surface. Besides, the control signals u_1 and u_2 can be obtained from the sliding surface.

First, we need to design an equilibrium surface. The sliding surface can be designed with errors of the dc-link voltage and the indirect component current of the PV system. Then, the sliding-mode manifold was defined as

$$S = \begin{bmatrix} s_1 \\ s_2 \end{bmatrix} = \begin{bmatrix} e_1 + \alpha_1 \int e_1 dt \\ \dot{e}_2 + \alpha_2 e_2 + \alpha_3 \int e_2 dt \end{bmatrix} \tag{26}$$

where $e_1 = y_1^* - y_1 = i_q^* - i_q$ and $e_2 = y_2^* - y_2 = v_{\rm dc}^* - v_{\rm dc}$. i_q^* reflects the desired power factor of the system. α_1 is the integral coefficient of the first-order error dynamics for e_1. For the requirement of stability, it should be ensuring that α_1 is greater than zero. Seminally, α_2 and α_3 are the proportionality coefficient and integral coefficient of the second-order error dynamics for e_2. It will be stable if $\alpha_2 > 0$ and $\alpha_3 > 0$. These three coefficients ensure the response speed and the oscillation magnitude of the system.

According to the sliding-mode control method, the state trajectory could keep on the sliding surface $S = \dot{S} = 0$. If (26) is substituted into $\dot{S} = 0$, it yields

$$\begin{cases} \dot{e}_1 = -\alpha_1 e_1 \\ \ddot{e}_2 = -\alpha_2 \dot{e}_2 - \alpha_3 e_2. \end{cases} \tag{27}$$

Equation (27) can constrain the system status (i_q and $v_{\rm dc}$) to follow the state trajectories which lie on a suitable surface in the sliding surface.

The next step is to design a control input which satisfies the sliding-mode existence law. The equivalent control is chosen to have the following structure:

$$u_i = u_{\rm ieq} + u_{\rm is} \tag{28}$$

where u_{ieq} is an equivalent control input which determines the behavior of the system on the sliding surface and u_{is} is a nonlinear switching input, which will keep the state variables on the sliding surface even if the parameters are changed and disturbed. The following can also be obtained by differentiating (26)

$$\begin{aligned} \dot{s}_1 &= \dot{e}_1 + \alpha_1 e_1 \\ &= \frac{1}{L}e_q - \frac{R}{L}i_q - \omega i_d - \frac{1}{L}u_2 + \lambda_1 \end{aligned} \tag{29}$$

$$\begin{aligned} \dot{s}_2 &= \ddot{e}_2 + \alpha_2 \dot{e}_2 + \alpha_3 e_2 \\ &= \frac{3e_d}{2Cv_{dc}}\left(\frac{1}{L}e_d - \frac{R}{L}i_d + \omega i_q - \frac{1}{L}u_1\right) \\ &\quad - \frac{3i_d e_d}{2Cv_{\rm dc}^2}\left(\frac{3}{2Cv_{\rm dc}}(e_d i_d) - \frac{1}{C}i_{\rm dc}\right) - \frac{1}{C}\dot{i}_{\rm dc} + \lambda_2 \end{aligned} \tag{30}$$

where $\lambda_1 = \dot{i}_q^* + \alpha_1 e_1$ and $\lambda_2 = \ddot{v}_{\rm dc}^* + \alpha_2 \dot{e}_2 + \alpha_3 e_2$. In the solution of $\dot{S} = 0$, the following equation is derived:

$$u_{1eq} = L\left(\frac{1}{L}e_q - \frac{R}{L}i_q - \omega i_d - \frac{1}{L}u_2 - \lambda_1\right) \tag{31}$$

$$\begin{aligned} u_{2eq} = \frac{2LCv_{\rm dc}}{3e_d}\Bigg[&\frac{3e_d}{2Cv_{\rm dc}}\left(\frac{1}{L}e_d - \frac{R}{L}i_d + \omega i_q - \frac{1}{L}u_1\right) \\ &- \frac{3i_d e_d}{2Cv_{\rm dc}^2}\left(\frac{3}{2Cv_{\rm dc}}(e_d i_d) - \frac{1}{C}i_{\rm dc}\right) - \frac{1}{C}\dot{i}_{\rm dc} - \lambda_2\Bigg]. \end{aligned} \tag{32}$$

Finally, the equivalent control laws are obtained to reduce the impact of parameter deviation.

$$\begin{cases} u_1 = u_{1eq} + u_{1s} = u_{1eq} + \beta_1 \text{sign}(s_1) \\ u_2 = u_{2eq} + u_{2s} = u_{2eq} + \beta_2 \text{sign}(s_2) \end{cases} \tag{33}$$

where β_1 and β_2 are positive constants. β_1 and β_2 are the parameters for system to overcome perturbation and external disturbance. The larger β_1 and β_2, the stronger the ability of the system to overcome parameter perturbation and external interference. However, the amplitude of the system oscillation is proportional to β_1 and β_2, and excessive gain will lead to the enhancement of the system oscillation.

Substituting (33) into (31) and (32) gives a result as follows:

$$\begin{cases} \dot{s}_1 = -\beta_1 \text{sign}(s_1) \\ \dot{s}_2 = -\beta_2 \text{sign}(s_2). \end{cases} \tag{34}$$

In order to verify the stability of the sliding-mode controller, Lyapunov function is chosen as

$$V = \frac{1}{2}S^T S. \tag{35}$$

Time derivative of Lyapunov function is computed as

$$\dot{V} = S^T \dot{S} = -\beta_1 |s_1| - \beta_2 |s_2| < 0. \tag{36}$$

Therefore, the proposed sliding-mode based feedback linearization controller can guarantee the system asymptotically stable and the system is input-output linearized. The mathematical steps to simulate the controller is shown in Fig. 7 after we explain the PV array operating point control method under the voltage dips.

C. PV Array Operating Point Control Under the Voltage Dips

In normal working condition, maximum power point tracking (MPPT) strategy is usually used in PV systems to obtain maximum grid-connected power. The dc-link reference voltage $v_{\rm dc}^*$ is generated by the MPPT function. In this article, the perturbation and observation method is used to realize MPPT due to its effectiveness and simplicity. In addition,

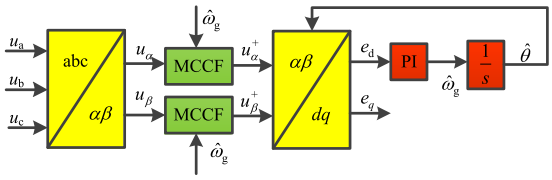

Fig. 5. Schematic diagram of the MCCF-PLL.

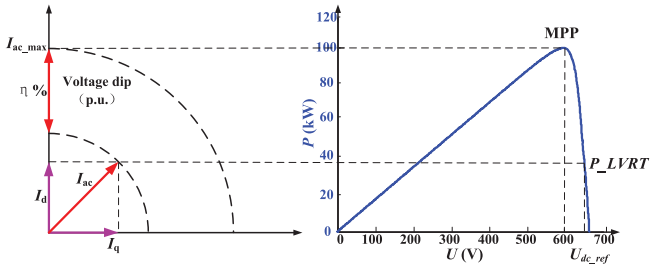

Fig. 6. Operation point selected method of the PV array under the grid dips.

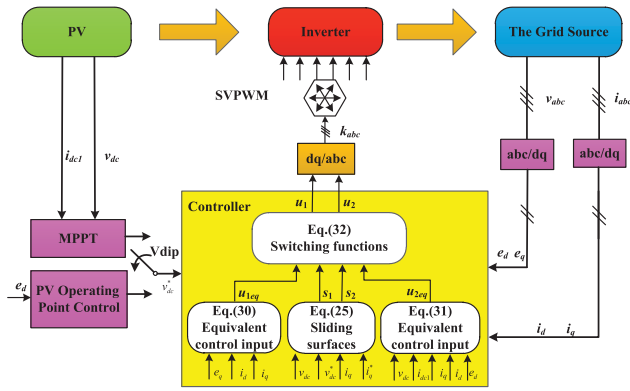

Fig. 7. Proposed control strategy for the central grid-connected PV system.

the multiple-complex coefficient-filter-based phase-locked loop (MCCF-PLL) is adopted [53], which is shown in Fig. 5. Based on traditional synchronous reference frame phase-locked loop (SRF-PLL), a MCCF filter is added in order to extract the sequence component e_d, e_q, and the angle of the grid voltage. Then, the MCCF-PLL could achieve fast and exact extraction even under asymmetric fault conditions. By detecting the e_d value, it can be determined whether a voltage dip fault has occurred. And the harmonics compensation, frequency, and the power quality could also be extracted using this method.

When a voltage dip occurs, the dc voltage and the ac currents will suddenly increase. Because the grid voltage dips cause the input and output power to be unbalanced, the change of ac currents and dc voltage is directly related to the depth of voltage dip.

The larger the depth, the greater the change. On the one hand, the response speed of the inverter must be increased to limit the increase of the ac current during the fall. The sliding-mode-based feedback linearization controller could obtain desired dynamic performances. Meanwhile, the PV panels should avoid continuing to work at the MPP. Changing the working point of the PV panels under LVRT is necessary to limit the transmission power.

The strategy adopted in this article is to select a suitable dc operating point to ensure the grid-connected current does not exceed the rated value. The dc operating point is selected based on the different depths of the grid drop and the reactive power requirements. The active and reactive power delivered to the grid could be given by

$$P = e_d i_d + e_q i_q \tag{37}$$

$$Q = e_d i_q - e_q i_d \tag{38}$$

where P is the active power and Q is the reactive power. Meanwhile, according to the instantaneous power balance theory, the energy transfer to the grid can be calculated

$$P = v_{\mathrm{dc}} i_{\mathrm{dc1}} = \frac{3}{2}(e_d i_d + e_q i_q). \tag{39}$$

The series resistance losses are neglected in this case. The instantaneous active power is the function of e_d. According to the law of power conservation, the ac-side currents will increase at the moment of voltage dip for the energy supplied by PV side remains unchanged.

If the drop depth of the voltage is $\eta\%$ of the rated grid voltage, the maximum power the system could transfer is

$$P = 3 \times (1 - \eta\%) \times v_{\mathrm{ac\_rated}} \times i_{\mathrm{ac\_max}} \times \cos\varphi \tag{40}$$

where $\cos\varphi$ is the power factor of the system. The greater the drop depth, the less power the system could handle. Based on the PV array model mentioned above, the P/V characteristics of PV array could obtain and the output current of the PV array can be calculated correctly. The grid-connected power after the voltage drop can be calculated by (40). If the PV operating point could be adjusted in time after detecting the voltage dips, the ac-side current stress will be effectively reduced. Therefore, we can select the dc-link reference voltage form the I/V and P/V characteristics of PV array, as shown in Fig. 6.

By limiting the duty cycle, the inverter could work in the right half plane of PV curve to prevent the system from bus voltage collapse. In addition, the stability margin on the right side has been elaborated in [55]. Thus, the stability margin on the right side of the PV characteristic could be obtained.

This operation point control method could ensure that the ac current is kept within the tolerance range. The ac-rated phase currents I_{rated} is 151 A in this system. It will be safe if the ac current is under 151 A when the LVRT occurs. Therefore, we choose the maximum phase currents value $I_{\mathrm{ac\_max}}$ equal to I_{rated}. The proposed control strategy is shown in Fig. 7.

D. DC-Link Capacitor Design Under Feedback Linearization Control

When adopting nonlinear control technology, the dc voltage capacity can be effectively reduced due to its fast control speed and fast response of the dc voltage [54]. For the PWM converter, the dc capacitor capacity is mainly selected according to the ripple current of the dc side of the system. When the capacitance is too large, the system cost and volume will increase. When the capacitance is too small, the capacitor may be burned down due

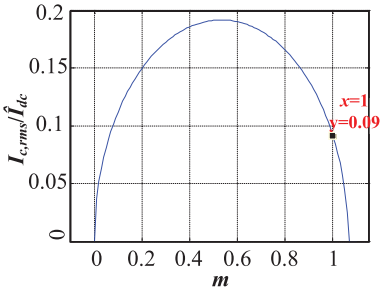

Fig. 8. Relationship between ripple current and modulation degree.

to the heating of the equivalent series resistance of the capacitor. The selection of dc capacitor should consider the modulation of the system and the speed of the system. For PWM converters, the rms of dc capacitor ripple current is

$$I_{c,\mathrm{rms}}^2 = m\hat{I}_{\mathrm{dc}}^2\left[\frac{\sqrt{3}}{4\pi} + \left(\frac{\sqrt{3}}{4} - \frac{9}{16}\right)m\right] \tag{41}$$

where $I_{c,\mathrm{rms}}$ is the rms of capacitive current, $\hat{I}_{\mathrm{dc}}$ is the peak value of input current, and m is the modulation degree. The dc capacitor ripple current depends on the modulation degree and the input current of the system

$$m = \frac{V_r}{\frac{v_{\mathrm{dc}}}{2}} \tag{42}$$

U_r is the peak ac voltage of the converter. In the *d–q* synchronous rotating coordinate system

$$U_r = \sqrt{U_g^2 + (\omega L i_d)^2}. \tag{43}$$

The relationship between dc capacitor ripple current and the modulation degree can be obtained.

When the modulation index is 1, the ratio of ripple current to peak current is 0.09, as shown in Fig. 8. Besides considering the dc capacitor ripple current, the response time of the system should also be considered. Assume that the system energy mutation mode is linear growth in a short time. The energy change of the system is

$$\Delta W_d \cong \frac{\Delta P_{\max} T_r}{2} \tag{44}$$

where $\Delta P_{\max}$ is the maximum transient power variation that the system can withstand within the safe range of dc voltage, and T_r is the response time of the system. We can also get that

$$\begin{aligned}\Delta W_d &\cong \frac{1}{2}C(U_2^2 - U_1^2) = \frac{1}{2}C(U_2 + U_1)(U_2 - U_1)\\ &\approx CU_{\mathrm{dc}}\Delta U_{\mathrm{dc}}\end{aligned} \tag{45}$$

where U_1 and U_2 are the dc voltage value before and after the power change, and the ΔU_{dc} is the dc voltage change value

$$C \geq \frac{\Delta P_{\max} T_r}{2U_{\mathrm{dc}}\Delta U_{\max}}. \tag{46}$$

The $\Delta U_{\max}$ is the maximum dc voltage change value that the system can withstand. The feedback linearization control system improved the response speed of the system by avoiding the delay caused by the integral link of the voltage and current PI regulator.

TABLE I
POWER STAGE PARAMETERS

Description	Value
Power ratings, P	100 kW
AC grid line voltage, U_{ac}	270V
The voltage of maximum power point, U_{mpp}	600V
Grid frequency f_g	50Hz
Switching frequency f_s	5 kHz
Transformer turns ratio, n	270/380
DC-link capacitance, C	5400 uF
AC inductance, L	1.5 mH

TABLE II
PARAMETERS COMPARISON OF THE CONTROLLERS

Parameter	PI	Feedback Linearization
Proportional coefficient of current loop, K_{IP}	0.7	0.5
Integral coefficient of current loop, K_{II}	2.0	1.5
Proportional coefficient of voltage loop, K_{VP}	1.5	1.2
Integral coefficient of voltage loop, K_{VI}	0.5	0.6

IV. SIMULATION AND EXPERIMENTAL VERIFICATIONS

The simulation of the single-stage central grid-connected PV inverter is carried out in MATLAB to verify the feasibility of the proposed sliding-mode-based feedback linearization control strategy. The power stage parameters of the system are shown in Table I.

The symmetric and asymmetric grid voltage dips are taken into consideration. The simulation time step is set to 1 ns, and the simulation conditions of the different cases are the same. It is assumed that the PV converter is under full-load condition and in the steady state before the grid dips, and the current overload capacity of the system is 1.2 times of the rated current. The parameters comparison of the controllers is listed in Table II.

The simulation results of symmetrical voltage dips are shown in Figs. 9–11. In Fig. 9(a), the drop depth of the voltage is 20% of the rated grid voltage, and the voltage drop depths of Figs. 10(a) and 11(a) are 50% and 80%, respectively. The grid voltage dips occur at $t = 0.3$ s and the grid voltage is restored to the rated value at $t = 0.4$ s. It can be noted that the current peak value was within the limit even under the fault, and the PV array operating point control was in action. As the grid dip occurs, the nonlinear feedback controller will track the desired working point of the PV model rapidly, as designed in Section III.

In order to verify the superiority of the proposed method, the performance of the traditional PI double-loop control is shown in Figs. 9(b)–11(b). The feedback linearization control method presents advantages in the instantaneous corresponding speed and tracking performance of dc-link voltage. It is due to the full relative degree obtained by feedback linearization technique.

The single-phase asymmetrical dips were also applied to the inverter, and the simulation results are shown in Fig. 12. In Fig. 12(a), the grid voltage drop depth of phase A is 20% of the rated grid voltage, and the other two-phase voltages remain

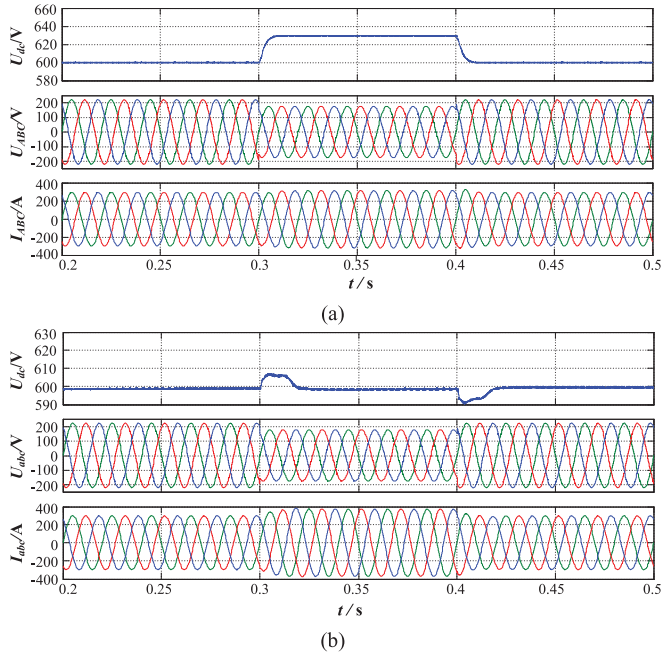

Fig. 9. Symmetrical dips waveforms with 20% depth of the rated grid voltage. (a) Sliding-mode based feedback linearization control. (b) Double-loop control.

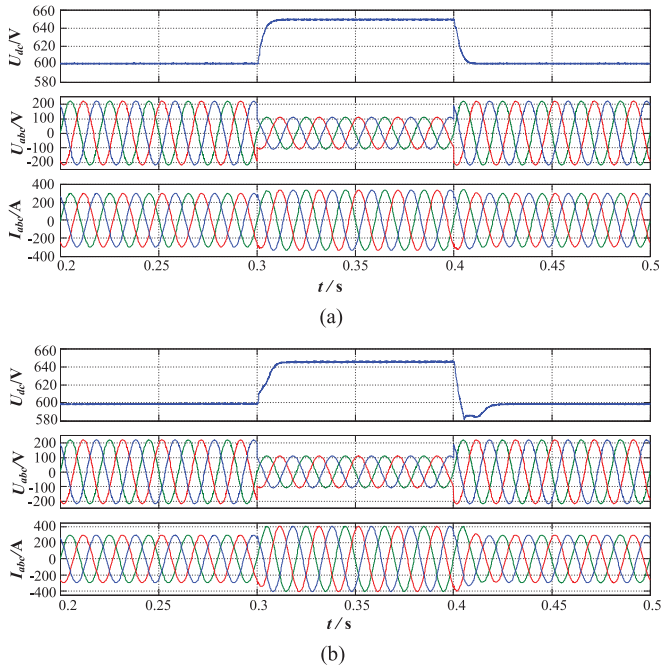

Fig. 10. Symmetrical dips waveforms with 50% depth of the rated grid voltage. (a) Sliding-mode-based feedback linearization control. (b) Double-loop control.

constant at rated voltages. Similarly, the voltage drop depth of Fig. 12(b) and (c) is 50% and 80%, respectively. The proposed control strategy also could realize reactive power support during the LVRT faults. The corresponding reactive power can be obtained by setting the i_q^*, which reflects the desired power factor of the system. To verify the reactive power support capability of the control system, the simulation of symmetrical voltage dips

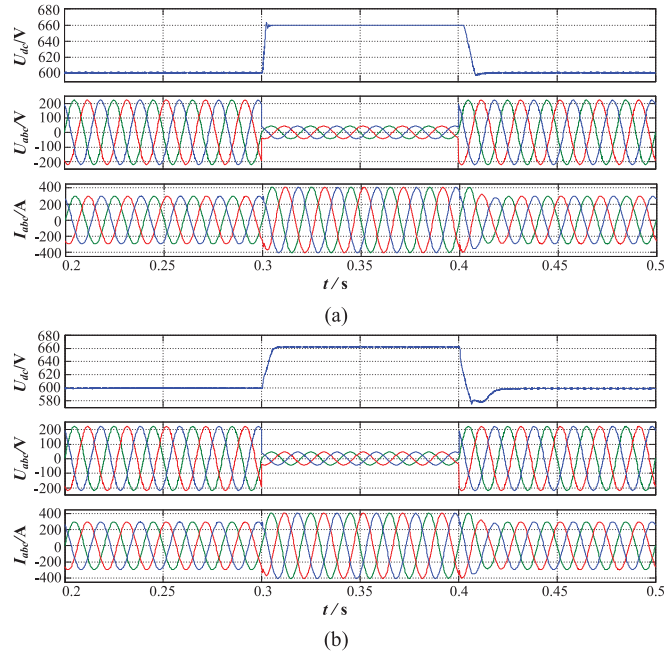

Fig. 11. Symmetrical dips waveforms with 80% depth of the rated grid voltage. (a) Sliding-mode-based feedback linearization control. (b) Double-loop control.

with reactive power support is given in Fig. 13. The drop depth of the voltage is 80% of the rated grid voltage, and the system injects 105% reactive current into the grid.

As the grid dip occurs, the nonlinear feedback controller will track the desired working point of the PV model rapidly, and the current peak value is within the limit of the system. In the case of asymmetric drops, it is still connected to the grid, which meets the requirements of the standard. However, the dc-link voltages are slightly oscillating under the asymmetrical grid dips, for the reference frame of dq0 control rotating in positive direction. In this case, the negative sequence of the voltage interacts with the positive sequence of the current. The proposed control strategy permits the inverter to operate in any fault situation without overcurrent as well as delivering sinusoidal current.

Usually, PV system has multiple inverters operating in parallel. To verify the effectiveness of this control strategy in multiple parallel operations, a simulation has been done. The simulation results of symmetrical voltage dips with three parallel units are shown in Fig. 14. In this simulation, there are three 100 kW PV inverters operating in parallel. The drop depth of the voltage is 80% of the rated grid voltage. Compared with single operation case, the oscillation of grid currents is slightly larger at the moment of voltage dip. The simulation results show that the control strategy can guarantee the stable operation of LVRT even in multiple parallel operations.

In order to verify robustness of the controller to the control parameters, the simulation of the control system with different ac inductance is carried out. The symmetrical dips waveforms based on different ac inductance L are shown in Fig. 15. In this simulation, only the value of ac inductance is changed. Inductance values are 0.5, 1.5, and 2.5 mH, respectively. The system can remain stable even if the ac inductance changes.

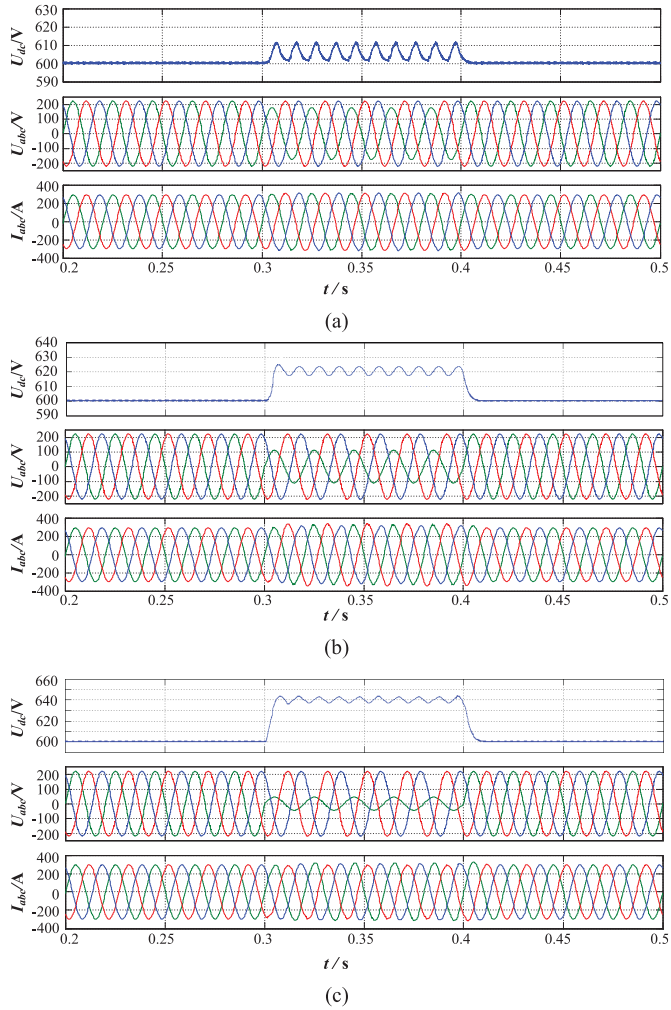

Fig. 12. Asymmetrical dips waveforms. (a) Grid voltage drop depth of phase A is 20% of the rated voltage. (b) Grid voltage drop depth of phase A is 50% of the rated voltage. (c) Grid voltage drop depth of phase A is 80% of the rated voltage.

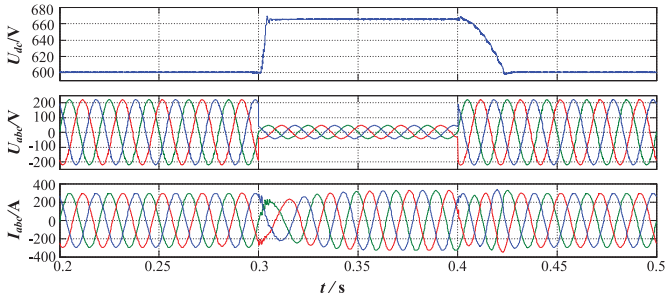

Fig. 13. Symmetrical dips waveforms with reactive power support.

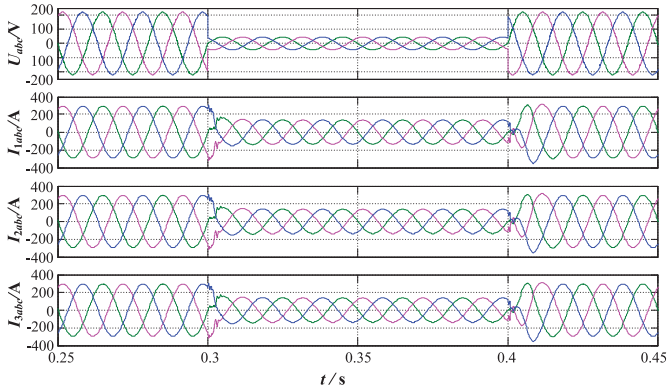

Fig. 14. Symmetrical dips waveforms of parallel operation.

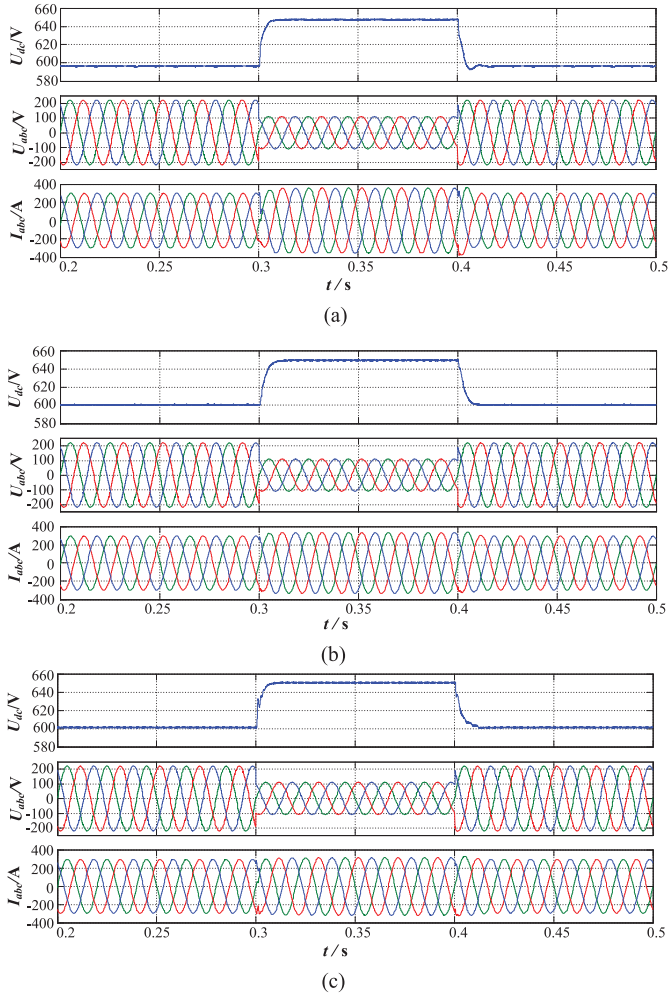

Fig. 15. Symmetrical dips waveforms based on different ac inductance L. (a) $L = 0.5$ mH. (b) $L = 1.5$ mH. (c) $L = 2.5$ mH.

A 100-kW prototype was built to verify the performance of the proposed control strategy. The nominal input dc voltage is designed at 600 V and the output ac voltage is fixed at 380 V for the PV connection. The transformer turns ratio is selected to be 270:380. The designed parameters are the same as the simulation, which is listed in Table I.

The experimental results provided below are based on the LVRT active test system. The real-time setup of the PV LVRT active test system is shown in Fig. 16. It contains the grid simulators, transformers, converter, IV simulator, and the tested inverter. The grid simulator can provide standard ac voltage of different types of LVRT grid dips. The ac–dc converter delivers

Fig. 16. Real-time setup of LVRT active test system.

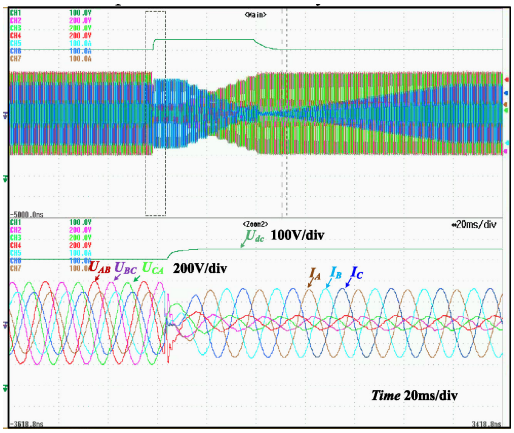

Fig. 17. Waveforms of line voltages and phase currents under grid voltage symmetrical dip to 20% of the rated grid voltage.

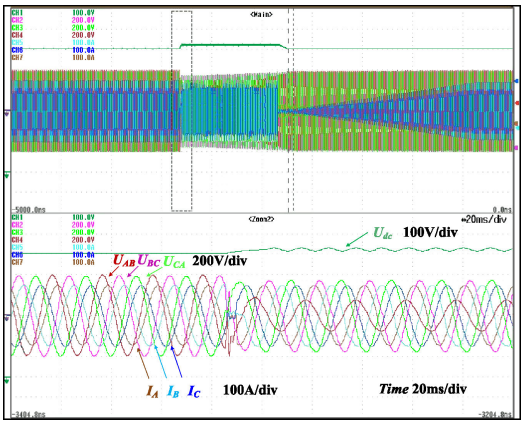

Fig. 18. Waveforms of line voltages and phase currents under grid voltage asymmetrical dip: phase A is 50% of the rated voltage.

the power to the IV simulator, and the IV simulator simulates the characteristic of the PV panels. In the experiment, the output load of the PV inverter is the grid simulator, and the input is the IV simulator.

In the following, three groups of experiment results are given. The experiment waveforms are shown in Figs. 17–19. Fig. 17 shows the experimental waveforms with the proposed sliding-mode-based feedback linearization control strategy under symmetric grid voltage dips, and the depth of the grid voltage

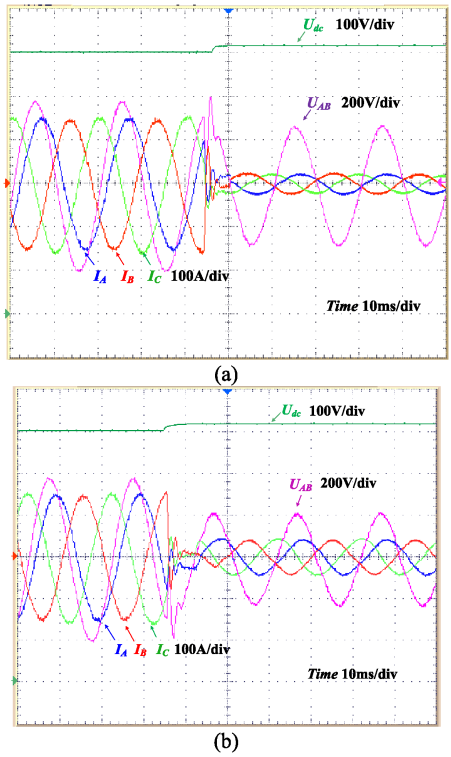

Fig. 19. Waveforms of line voltages and phase currents under grid voltage symmetrical dip to 20% at different phase angles. (a) Symmetrical voltage dip occurs at the $\pi/2$ degrees of the line voltage U_{AB}. (b) Symmetrical voltage dip occurs at the $3\pi/2$ degrees of the line voltage U_{AB}.

is 80% of the rated voltage. Fig. 18 shows the experimental waveforms with the proposed feedback linearization control strategy under asymmetric grid voltage dips, and the depth of the grid voltage is 50% of the rated voltage.

Before the grid voltage dips, the output ac current of the system is maintained at 175 A. When a grid dip occurs, the system ac current is quickly suppressed, and there is no ac current surge at the time of the rapid fall, and the dc voltage rapidly rises to a steady state. As the grid pressure enters the dip steady state, the system output current remains constant and continues to deliver power to the grid. Similar to nominal input voltage conditions, the ac current is within the limit of the system and it is sinusoidal under the grid dip. When the grid voltage returns to normal, the system ac current also returns to the rated value and the system power restores to the rated power with the power change rate of 30 kW/s.

Since the dip at the peak voltage has the greatest impact on the inverter, the experimental results of positive and negative peak voltage dips are given in Fig. 19. As the grid dip occurs, the nonlinear feedback controller will track the desired working point of the PV model rapidly to ensure the system works properly. It can be seen that the proposed feedback linearization control strategy improves the system response speed and has a significant improvement on the system voltage safety and stability.

The traditional PI double-loop control strategy comparison tests are also given as shown in Fig. 20. The waveform under

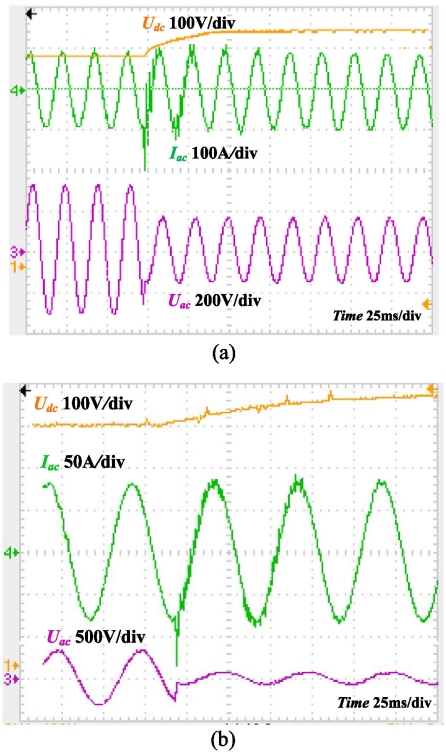

Fig. 20. Waveforms of line voltages and phase currents under grid voltage symmetrical dip with the traditional PI double-loop control method. (a) Grid voltage symmetrical dip to 50% of the rated grid voltage at 50% load. (b) Grid voltage symmetrical dip to 20% of the rated grid voltage at 50% load.

grid voltage symmetrical dip to 50% of the rated grid voltage at 50% load is shown in Fig. 20(a). As you can see, the system may have short-term overcurrent in practical application due to adjusting speed of the controller and the power imbalance at the moment of the voltage dips. Additionally, the waveform under the grid voltage symmetrical drop to 20% of the rated grid voltage at 50% load is also given in Fig. 20(b). In this test, we add the PV operating point control method to the controller, which will decrease the power imbalance at the moment of the voltage dips. However, the overcurrent spike is still large for the deep drop and the heavy load, which is unfavorable for the system. Compared with the traditional PI double-loop control strategy, the feedback linearization control method has advantages in the instantaneous corresponding speed and tracking performance due to the full relative degree.

V. Conclusion

In this article, a sliding-mode-based feedback linearization control strategy is proposed for PV inverter in LVRT applications. The proposed control strategy ensures that the inverter not only keeps the benefits under the normal working condition, but also achieves a wide-range regulation ability and faster response while operating under the LVRT condition. The proposed control strategy has the following distinct features:

1) Completed decoupling and linearization over the entire operating range and fast dynamic response of LVRT are realized through the proposed approach.
2) The proposed PV array operating point control under the voltage dip reduces the imbalance of the input and output power during the LVRT. Thus, the overshoot ac current during transitions will be reduced.
3) Compared to the conventional dual-loop PI control, the proposed control strategy guarantees the desired dynamic response and robustness performance while operating under both symmetrical and asymmetrical LVRT conditions.

References

[1] Global Market Outlook for Solar Power 2017–2021, the Solar Power Europe, 2017. [Online]. Available: http://www.solarpowereurope. org/reports/global-market-outlook-2017
[2] Solar debt financing on pace to reach highest since 2010, the Bloomberg New Energy Finance (BNEF), 2014. [Online]. Available: http://www.bnef.org
[3] M. Ding, Z. Xu, W. Wang, X. Wang, Y. Song, and D. Chen, "A review on China's large-scale PV integration: Progress, challenges and recommendations," *Renewable Sustain. Energy Rev.*, vol. 53, pp. 639–652, Jan. 2016.
[4] J. S. Kim, J. M. Kwon, and B. H. Kwon, "High-efficiency two-stage three-level grid-connected photovoltaic inverter," *IEEE Trans. Ind. Electron.*, vol. 65, no. 3, pp. 2368–2377, Mar. 2018.
[5] C. T. Lee, C. W. Hsu, and P. T. Cheng, "A low-voltage ride through technique for grid connected converters of distributed energy resources," *IEEE Trans. Ind Appl.*, vol. 47, no. 4, pp. 1821–1832, Jul.–Aug. 2011.
[6] The Grid Code, High and Extra High Voltage, E. ON Netz GmbH, Bayreuth, Germany, Jul. 2010. [Online]. Available: http://www.eon-netz.com
[7] *The Grid Code, Issue 4 Revision* 2, Nat. Grid Elect. Transm. plc, U.K., Mar. 2010. [Online]. Available: http://www.nationalgrid.com/uk
[8] State grid corporation of China, *Q/GDW617/-2011*, "Technical rule for photovoltaic power station connected to power grid," China Electric Power Press, Beijing, China, Mar. 2011.
[9] S. Yang, Q. Lei, F. Z. Peng, and Z. Qian, "A robust control scheme for grid-connected voltage-source inverters," *IEEE Trans. Ind. Electron.*, vol. 58, no. 1, pp. 202–212, Jan. 2011.
[10] X. Zhao, L. Zhang, R. Born, and J.-S. Lai, "A high-efficiency hybrid resonant converter with wide-input regulation for photovoltaic applications," *IEEE Trans. Ind. Electron.*, vol. 65, no. 5, pp. 3684–3695, May 2017.
[11] L. Zhang *et al.*, "A sensorless implementation of the parabolic current control for single-phase stand-alone inverters," *IEEE Trans. Power Electron.*, vol. 31, no. 5, pp. 3913–3921, Aug. 2016.
[12] S. Kwak and J.-C. Park, "Predictive control method with future zero-sequence voltage to reduce switching losses in three-phase voltage source inverters," *IEEE Trans. Power Electron.*, vol. 30, no. 3, pp. 1558–1566, Mar. 2015.
[13] G.-Y. Gu, L.-M. Zhu, and C.-Y. Su, "Modeling and compensation of asymmetric hysteresis nonlinearity for piezoceramic actuators with a modified Prandtl–Ishlinskii model," *IEEE Trans. Ind. Electron.*, vol. 61, no. 3, pp. 1583–1595, Mar. 2014.
[14] Y. Yang, F. Blaabjerg, and H. Wang, "Low-voltage ride-through of single-phase transformerless photovoltaic inverters," *IEEE Trans. Ind Appl.*, vol. 50, no. 3, pp. 1942–1952, May–Jun. 2014.
[15] Z. Shao *et al.*, "Analysis and control of neutral-point voltage for transformerless three-level PV inverter in LVRT operation," *IEEE Trans. Power Electron.*, vol. 32, no. 3, pp. 2347–2359, Mar. 2017.
[16] C. Y. Tang, Y. T. Chen, and Y. M. Chen, "PV power system with multimode operation and low-voltage ride-through capability," *IEEE Trans. Ind. Electron.*, vol. 62, no. 12, pp. 7524–7533, Dec. 2015.
[17] C. H. Benz, W.-T. Franke, and F. W. Fuchs, "Low voltage ride through capability of a 5 kW grid-tied solar inverter," in *Proc. Int. Power Electron. Motion Control Conf.*, Ohrid, 2010, pp. T12-13–T12-20.
[18] Y. Zhang, Y. Lu, and T. Q. Zheng, "Optimization and design of LVRT strategy of photovoltaic grid-connected system," *Trans. China Electrotechnical Soc.*, vol. 28, no. 12, pp. 136–141, Dec. 2013.
[19] A. Junyent-Ferre, O. Gomis-Bellmunt, T. C. Green, and D. E. Soto-Sanchez, "Current control reference calculation issues for the operation of renewable source grid interface VSCs under unbalanced voltage sags," *IEEE Trans. Power Electron*., vol. 26, no. 12, pp. 3744–3753, Dec. 2011.
[20] N. Kumar, T. K. Saha, and J. Dey, "Sliding-mode control of PWM dual inverter-based grid-connected PV system: Modeling and performance analysis," *IEEE J. Emerg. Sel. Topics Power Electron.*, vol. 4, no. 2, pp. 435–444, Jun. 2016.

[21] I.-S. Kim, "Robust maximum power point tracker using sliding mode controller for the three-phase grid-connected photovoltaic system," *Sol. Energy*, vol. 81, no. 3, pp. 405–414, Mar. 2007.
[22] C.-C. Chu and C.-L. Chen, "Robust maximum power point tracking method for photovoltaic cells: A sliding mode control approach," *Sol. Energy*, vol. 83, no. 8, pp. 1370–1378, Aug. 2009.
[23] Y.-K. Chen, C.-H. Yang, and Y.-C. Wu, "Robust fuzzy controlled photovoltaic power inverter with Taguchi method," *IEEE Trans. Aerosp. Electron. Syst.*, vol. 38, no. 3, pp. 940–954, Jul. 2002.
[24] M. A. Hannan, Z. A. Ghani, M. M. Hoque, P. J. Ker, A. Hussain, and A. Mohamed, "Fuzzy logic inverter controller in photovoltaic applications: Issues and recommendations," *IEEE Access*, vol. 7, pp. 24934–24955, Feb. 2019.
[25] B. N. Alajmi, K. H. Ahmed, S. J. Finney, and B. W. Williams, "Fuzzy-logic-control approach of a modified hill-climbing method for maximum power point in microgrid standalone photovoltaic system," *IEEE Trans. Power Electron.*, vol. 26, no. 4, pp. 1022–1030, Apr. 2011.
[26] A. Merabet, L. Labib, A. M. Y. M. Ghias, C. Ghenai, and T. Salameh, "Robust feedback linearizing control with sliding mode compensation for a grid-connected photovoltaic inverter system under unbalanced grid voltages," *IEEE J. Photovolt.*, vol. 7, no. 3, pp. 828–838, May 2017.
[27] A. Mojallal and S. Lotfifard, "Enhancement of grid connected PV arrays fault ride through and post fault recovery performance," *IEEE Trans. Smart Grid*, vol. 10, no. 1, pp. 546–555, Jan. 2019.
[28] H. M. Hasanien, "An adaptive control strategy for low voltage ride through capability enhancement of grid-connected photovoltaic power plants," *IEEE Trans. Power Syst.*, vol. 31, no. 4, pp. 3230–3237, Jul. 2016.
[29] A. Moghadasi, A. Sargolzaei, A. Anzalchi, M. Moghaddami, A. Khalilnejad, and A. Sarwat, "A model predictive power control approach for a three-phase single-stage grid-tied PV module-integrated converter," *IEEE Trans. Ind Appl.*, vol. 54, no. 2, pp. 1823–1831, Mar.–Apr. 2018.
[30] M. Easley, S. Jain, M. B. Shadmand, and H. Abu-Rub, "Computationally efficient distributed predictive controller for cascaded multilevel impedance source inverter with LVRT capability," *IEEE Access*, vol. 7, pp. 35731–35742, Mar. 2019.
[31] G. Ding *et al.*, "Adaptive DC-link voltage control of two-stage photovoltaic inverter during low voltage ride-through operation," *IEEE Trans. Power Electron.*, vol. 31, no. 6, pp. 4182–4194, Jun. 2016.
[32] Y. W. Li, F. Blaabjerg, D. M. Vilathgamuwa, and P. C. Loh, "Design and comparison of high performance stationary-frame controllers for DVR implementation," *IEEE Trans. Power Electron.*, vol. 22, no. 2, pp. 602–612, Mar. 2007.
[33] Y. Zhang, L. Zhou, M. Sumner, and P. Wang, "Single-switch, wide voltage-gain range, boost dc–dc converter for fuel cell vehicles," *IEEE Trans. Veh. Technol.*, vol. 67, no. 1, pp. 134–145, Jan. 2018.
[34] Y. S. Choi, H. H. Choi, and J. W. Jung, "Feedback linearization direct torque control with reduced torque and flux ripples for IPMSM drives," *IEEE Trans. Power Electron.*, vol. 31, no. 5, pp. 3728–3737, May 2016.
[35] K. H. Kim, Y. C. Jeung, D. C. Lee, and H. G. Kim, "LVRT scheme of PMSG wind power system based on feedback linearization," *IEEE Trans. Power Electron.*, vol. 27, no. 5, pp. 2376–2384, May 2012.
[36] X. Bao, F. Zhuo, Y. Tian, and P. Tan, "Simplified feedback linearization control of three-phase photovoltaic inverter with an LCL filter," *IEEE Trans. Power Electron.*, vol. 23, no. 3, pp. 2739–2752, Jun. 2013.
[37] Y. Zhang, L. Ma, and T. Q. Zheng, "Application of feedback linearization strategy in voltage fault ride-through for photovoltaic inverters," in *Proc. IEEE Conf. Ind. Electron. Soc.*, Oct. 20111, pp. 4666–4671.
[38] A. O. Zue and A. Chandra, "State feedback linearization control of a grid connected photovoltaic interface with MPPT," in *Proc. IEEE Electr. Power Energy Conf.*, Montreal, QC, Oct. 2009, pp. 1–6.
[39] D. Lalili, A. Mellit, N. Lourci, B. Medjahed, and E. M. Berkouk, "Input output feedback linearization control and variable step size MPPT algorithm of a grid-connected photovoltaic inverter," *Renewable Energy*, vol. 36, no. 12, pp. 3282–3291, Dec. 2011.
[40] F. Delfino, G. B. Denegri, M. Invernizzi, and R. Procopio, "Feedback linearisation oriented approach to Q-V control of grid connected photovoltaic units," *IET Renewable Power Gener.*, vol. 6, no. 5, pp. 324–339, 2012.
[41] J. Matas, M. Castilla, J. M. Guerrero, L. G. de Vicuna, and J. Miret, "Feedback linearization of direct-drive synchronous wind-turbines via a sliding mode approach," *IEEE Trans. Power Electron.*, vol. 23, no. 3, pp. 1093–1103, May 2008.
[42] L. Callegaro, M. Ciobotaru, D. J. Pagano, and J. E. Fletcher, "Feedback linearization control in photovoltaic module integrated converters," *IEEE Trans. Power Electron.*, vol. 34, no. 7, pp. 6876–6889, Jul. 2019.
[43] R. Errouissi and A. Al-Durra, "Disturbance–observer-based control for dual-stage grid-tied photovoltaic system under unbalanced grid voltages," *IEEE Trans. Ind. Electron.*, vol. 66, no. 11, pp. 8925–8936, Nov. 2019.
[44] F. Lin, K. Lu, T. Ke, B. Yang, and Y. Chang, "Reactive power control of three-phase grid-connected PV system during grid faults using takagi-sugeno-kang probabilistic fuzzy neural network control," *IEEE Trans. Ind. Electron.*, vol. 62, no. 9, pp. 5516–5528, Sep. 2015.
[45] D. Fan, Y. Wang, S. Hu, M. Chen, and X. He, "Modeling and state-space feedback design of the battery current controller for the energy stored quasi-Z-source inverter," in *Proc. IEEE Energy Convers. Congr. Expo.*, Cincinnati, OH, USA, 2017, pp. 5159–5163.
[46] M. A. Mahmud, H. R. Pota, and M. J. Hossain, "Dynamic stability of three-phase grid-connected photovoltaic system using zero dynamic design approach," *IEEE J. Photovolt.*, vol. 2, no. 4, pp. 564–571, Oct. 2012.
[47] J. Morren and S. W. H. Haan, "Ride through of wind turbines with doubly-fed induction generator during a voltage dip," *IEEE Trans. Energy Convers.*, vol. 20, no. 2, pp. 435–441, Jun. 2005.
[48] V. Ignatova, P. Granjon, and S. Bacha, "Space vector method for voltage dips and swells analysis," *IEEE Trans. Power Del.*, vol. 24, no. 4, pp. 2054–2061, Oct. 2009.
[49] M. H. J. Bollen, *Understanding Power Quality Problems-Voltage Sags & Interruptions*. New York, NY, USA: Wiley, 2000.
[50] IEEE recommended practice for voltage sag and short interruption ride-through testing for end-use electrical equipment eated less than 1000 V, in IEEE Std 1668-2017 (Revision of IEEE Std 1668-2014), 27 Nov. 2017.
[51] J. Lewis Blackburn, *Symmetrical Components for Power Systems Engineering*. New York, NY, USA: Marcel Dekker, 1993.
[52] S. Sastry, *Nonlinear Systems: Analysis, Stability and Control*. Berlin, Germany: Springer, 1999.
[53] X. Guo, W. Wu, and Z. Chen, "Multiple-complex coefficient-filter-based phase-locked loop and synchronization technique for three-phase grid interfaced converters in distributed utility networks," *IEEE Trans. Ind. Electron.*, vol. 58, no. 4, pp. 1194–1204, Apr. 2011.
[54] L. Malesani, L. Rossetto, P. Tenti, and P. Tomasin, "AC/DC/AC PWM converter with reduced energy storage in the DC link," *IEEE Trans. Ind Appl.*, vol. 31, no. 2, pp. 287–292, Mar.–Apr. 1995.
[55] M. A. Mahmud, M. J. Hossain, and H. R. Pota, "Dynamic stability analysis of photovoltaic cell using Lyapunov functions," in *Proc. 48th Annu. Conf. Australian Solar Energy Soc.*, Mawson, 2010, pp. 1–9.

Yajing Zhang was born in Hebei, China, in 1984. She received the B.S. and Ph.D. degrees in electrical engineering from Beijing Jiaotong University, China, in 2008 and 2015, respectively.

From February 2015 to August 2017, she was a Postdoctoral Fellow in control science and engineering with the Beijing University of Chemical Technology, China. Since 2017, she has been a Lecturer with the College of Automation, Beijing Information and Science Technology University, Beijing, China. Her current research interests include high-efficiency dc–dc converters, high-power density dc–dc converters, and renewable energy applications.

Jing Wang was born in Henan, China, in 1986. She received the M.S. degree from the Department of Electrical Engineering, Huazhong University of Science and Technology, Wuhan, China, in 2012.

She is currently working with Shenzhen Power Supply Bureau Co., Ltd. Her current research interests include power system analysis and dc technology.

Hong Li (Senior Member, IEEE) received the B.Sc., M.Sc., and Ph.D. degrees from the Taiyuan University of Technology, South China University of Technology, and Fernuniversitaet, Hagen, Germany, in 2002, 2005, and 2009, respectively.

She is currently a Professor with the School of Electrical Engineering, Beijing Jiaotong University, Beijing, China. She has authored/coauthored one book, 30 journal articles, and 39 conference papers. She has also applied for 20 patents. Her research interests include nonlinear modeling, analysis, and its applications, EMI suppressing methods for power electronic systems, as well as wide-bandgap power devices and applications.

Dr. Li is the Vice-Chairman of the Electromagnetic Compatibility Specialized Committee at the China Power Supply Society. She is an Associate Editor of the IEEE TRANSACTIONS ON INDUSTRIAL ELECTRONICS, and an Associate Editor of the *Chinese Journal of Electrical Engineering*.

Trillion Q. Zheng (Senior Member, IEEE) was born in Jiangshan, Zhejiang Province, China, in 1964. He received the B.S. degree from Southwest Jiaotong University, Sichuan, China, in 1986, and the M.S. and Ph.D. degrees from Beijing Jiaotong University, Beijing, China, in 1992 and 2002, respectively, all in electrical engineering.

He is a University Distinguished Professor with Beijing Jiaotong University. He is the Director of the Center for Electric Traction, sponsored by the Ministry of Education, China. He holds 24 Chinese patents and has authored/coauthored over 80 journal articles and more than 120 technical papers in conference proceedings. From 2003 to 2011, he served as Dean of the School of Electrical Engineering, Beijing Jiaotong University. He is serving as the Deputy Director of the Beijing Society for Power Electronics. His current research interests include the power supplies and ac drives of railway traction systems, high-performance and low-loss power electronics systems, and power quality corrections.

Dr. Zheng was a Laureate of the Delta Scholar for Power Electronics and Motor Drives of the Delta Environmental and Educational Foundation and received many other provisional-level and national-level awards.

Jih-Sheng Lai (Life Fellow, IEEE) received the M.S. and Ph.D. degrees in electrical engineering from the University of Tennessee, Knoxville, in 1985 and 1989, respectively.

In 1989, he joined the Electric Power Research Institute (EPRI) Power Electronics Applications Center (PEAC), where he managed EPRI-sponsored power electronics research projects. In 1993, he then joined the Oak Ridge National Laboratory, as Power Electronics Lead Scientist, where he initiated a high-power electronics program and developed several novel high-power converters including multilevel converters and soft-switching inverters. In 1996, he joined the Virginia Polytechnic Institute and State University. Currently, he is the James S. Tucker Professor with Electrical and Computer Engineering Department and Director of Future Energy Electronics Center. He has authored/coauthored more than 470 refereed technical papers, one book chapter, two books, and 29 patents. His main research interests include high-efficiency power electronics conversions for high power and energy applications.

Dr. Lai received Technical Achievement Award in Lockheed Martin Award Night, two Journal Paper Awards, and 13 Best Paper Awards from IEEE-sponsored conferences. He was the recipient of 2016 IEEE IAS Gerald Kliman Innovator Award. He led the student teams to win the Top Three Finalist in Google Little Box Challenge in 2016, Grand Prize Award from International Future Energy Challenge (IFEC) in 2011, and Grand Prize Award from Texas Instruments Engibous Analog Design Competition in 2009. He is the Founding Chair of 2001 IEEE IFEC and 2016 IEEE ACEPT, General Chair of IEEE COMPEL-2000, IEEE APEC 2005, IEEE SPEC-2018, and IEEE IFEEC-2019 conferences.

Jianguo Li was born in Hebei, China, in 1975. He received the B.S. degree from the Department of Electrical Engineering, North China Electric Power University, Baoding, China, in 1997, the M.S. degree from the Department of Electrical Engineering, Tsinghua University, Beijing, China, in 2005, and the Ph.D. degree from the College of Electrical and Electronic Engineering, North China Electric Power University, Beijing, in 2017.

He is currently an Associate Professor with the College of Automation, Beijing Information Science and Technology University, Beijing.

His current research interests include bidirectional dc–dc converter, high-frequency-link power conversion system, and flexible ac and dc transmission or distribution system.

Jiuhe Wang was born in Jilin, China. He received the B.S. degree from the School of Electrical and Control, Liaoning Technical University, Fuxin, China, in 1982, and the Ph.D. degree from the School of Information Engineering, University of Science and Technology Beijing, Beijing, China, in 2005.

He is currently a Professor with the School of Automation, Beijing Information Science and Technology University, Beijing. His current research interests include nonlinear control of power electronics converter, power quality control, and microgrids.

Qian Chen was born in Zhejiang Province, China, in 1987. He received the B.S. and Ph.D. degrees in electrical engineering from Beijing Jiao Tong University, Beijing, China, in 2009 and 2015, respectively.

He is currently an Engineer with the Zhejiang Electric Power Corporation Research Institute, Hang Zhou, China. His current research interests include HVdc, FACTS, and dc grids.